We are IntechOpen, the world's leading publisher of Open Access books
Built by scientists, for scientists

4,800
Open access books available

122,000
International authors and editors

135M
Downloads

154
Countries delivered to

Our authors are among the

TOP 1%
most cited scientists

12.2%
Contributors from top 500 universities

CLARIVATE ANALYTICS
BOOK CITATION INDEX
INDEXED

WEB OF SCIENCE™

Selection of our books indexed in the Book Citation Index
in Web of Science™ Core Collection (BKCI)

Interested in publishing with us?
Contact book.department@intechopen.com

Numbers displayed above are based on latest data collected.
For more information visit www.intechopen.com

On the Behavior of Ni Magnetic Nanowires as Studied by FMR and the Effect of "Blocking"

Carlos A. Ramos[1], Ettore C. Vassallo Brigneti[1],
Emilio De Biasi[1] and Manuel Vázquez[2]
[1]Centro Atómico Bariloche e Instituto Balseiro,
Universidad Nacional de Cuyo, Rio Negro,
[2]Instituto de Ciencias de Materiales, CSIC, Madrid
[1]Argentina
[2]Spain

1. Introduction

The development of nano-patterned membranes and nanowires (NW) is based on the interest in basic and applied research ranging from spintronics [Fert, 2008], chemical [Casanova *et al.*, 2008], biosensing [Orosco *et al.*, 2009; Pacholski *et al.*, 2006], semiconductor [Yang, *et al.*, 2010] and microwave applications [Darques *et al.*, 2009] among others [Ferain & Legras, 2009]. In particular, the study and applications of NWs has grown extensively during the last decades. One possibility to fabricate NWs is based on electron beam lithography leading to well defined structures of no less than ~100nm lateral size. In contrast with this technique there are other possibilities to generate nanoporous templates based on chemical or in physicochemical techniques [Pirota *et al.*, 2010]. One of these uses energetic heavy-ion particle beams impinging on a polymer membrane and subsequent chemical etching [Fert & Piraux, 1999]. Such membranes are commercially available with varying diameters and pore-density. Also a two-step anodization process [Masuda & Fukuda, 1995; Nielsch *et al.*, 2001] of aluminum leads to self-organized pores of amorphous anodized aluminum oxide (AAO) with a hexagonal order over relatively large regions (1-2μm). The pores align perpendicular to the substrate and remain separated from each other. These AAO templates can be prepared using different solutions and conditions of anodization, leading to varying diameters (20nm -110 nm), separation (65 - 500nm), and degree of order [Niesch *et al.*, 2001; Vázquez *et al*, 2004]. These templates were used for growing by electrodeposition the Ni NWs that are the subject of this chapter.

Ferromagnetic NW can be approximated as uniformly magnetized single domains with reversal mechanisms that depend on the wire diameter [Hertel & Kirschner, 2004]. The magnetic characteristic of a NW array depends crucially on its effective anisotropy. The anisotropy measurement, its origin, and possible ways of modifying it, are of large interest in basic research and applications.

For the characterization of magnetic NWs arrays ferromagnetic resonance (FMR) is an excellent technique as it yields direct information about the uniform precession mode

which can be related to the average anisotropy magnitude [De La Torre Medina *et al.*, 2010; Encinas-Oropesa *et al.*, 2001; Ramos *et al.*, 2004a; 2004b]. Its variation on the sample that may be related to anisotropy fluctuations and/or to other relaxation routes. Other excitations, related to spin-waves or surface modes can also be studied by FMR in nanowires [Kraus *et al.*, 2011].

In the present chapter we deal with some of the relevant aspects associated to FMR studies of NW arrays. We will start describing briefly the preparation method, its structural characterization, the magnetic characterization (Scanning Electron Microscopy, SEM, Atomic Force Microscopy, AFM, and X-ray diffraction, dc Magnetometry, Magnetic Force Microscopy, MFM, and FMR). In this sense we will show how the magnetic anisotropy is extracted from the experiment, the information involved in the linewidth regarding alignment and order/disorder contribution.

Magnetic Nanoparticles (MNPs) manifest a crossover from superparamagnetic-regime to blocked-regime which is observed at low temperatures and low fields, when the magnetic anisotropy barrier becomes comparable with the thermal fluctuation energy within a time-interval of measurement [Brown, 1963]. As magnetic NWs have a magnetic anisotropy much larger than the thermal energy, they represent ideal systems to study FMR in "blocked" systems, in the same sense this word is used for MNPs. Indeed, all particles with a substantial uniaxial anisotropy should behave in a very similar way to this magnetic NW as long as they can be considered as single-domain, which is a characteristic of small MNPs. As there has been many publications pointing to the effect this "blocking" has on the FMR spectra in MNPs we will treat these concepts relating the NW magnetization and FMR of these model systems. In doing this we hope to contribute to understand the relation between "blocking" and its effect on the FMR spectra.

2. Sample preparation and characterization

Highly-ordered AAO membranes were prepared by two-step anodization process of a high purity Al foil [Masuda & Fukuda, 1995]. In this way it is obtained a self-organized nanostructured template with high density of uniform parallel cylindrical pores aligned perpendicular to the surface. Varying the anodizing conditions the pore diameters can be changed between roughly 10 and 200 nm. Except otherwise indicated the anodization of the samples presented here was performed in a 0.3 M oxalic acid solution at 2ºC temperature under an applied potential of 40 V. A two-step anodization process allows us to obtain large scale polycrystalline array of the nanopores. (Fig. 1) The first anodization step in our samples lasted 24h (SNi) and 3h (SA) and is schematically drawn in Fig. 1b. This first AAO is eliminated by chemical etching of the AAO and the Al is exposed to a second anodization step performed for a few hours to produce the desired AAO template. The AAO obtained is then characterized by the presence of an array of self-ordered nanopores with a diameter of ~ 35 nm arranged in a dense hexagonal lattice with a parameter ~ 105 nm. The length of the nanopores, depends on the second anodization step duration. The AAO is then used as a template for the growth of the metallic NW by electrodeposition. However, the presence of an insulating alumina barrier-layer at the bottom of each nanopore prevents a direct deposition of material. Therefore, a suitable chemical process is used to reduce the thickness of the barrier-layer, resulting in the formation of dendrites, thus enabling the subsequent filling of pores with Ni by a pulsed-

electrodeposition method. Details regarding the electrodeposition conditions are given in the literature [Nielsch *et al*, 2000; 2001; Pirota *et al* 2004; Vázquez *et al*, 2004].

The pore filling-factor in the untreated AAO is close to 10% and can be increased by chemical treatments. Using pulsed electrodeposition these nanopores can be filled with a magnetic (Fe, Co, Ni) or non-magnetic metal. For this chapter we will deal with electrodeposited Ni NWs of typical legths 3µm (SNi) and 1 µm (SA). The typical aspect ratio (length/diameter) are close 80 (SNi) and 30 (SA). Ni NWs have a very small crystalline anisotropy as compared to the shape anisotropy which is, in magnetic field units, close 3 kOe for large aspect ratios (the shape anisotropy saturates rapidly for aspect ratios larger than 5[Cullity 1972]). This relatively small anisotropy field makes these samples very suitable for studying with FMR.
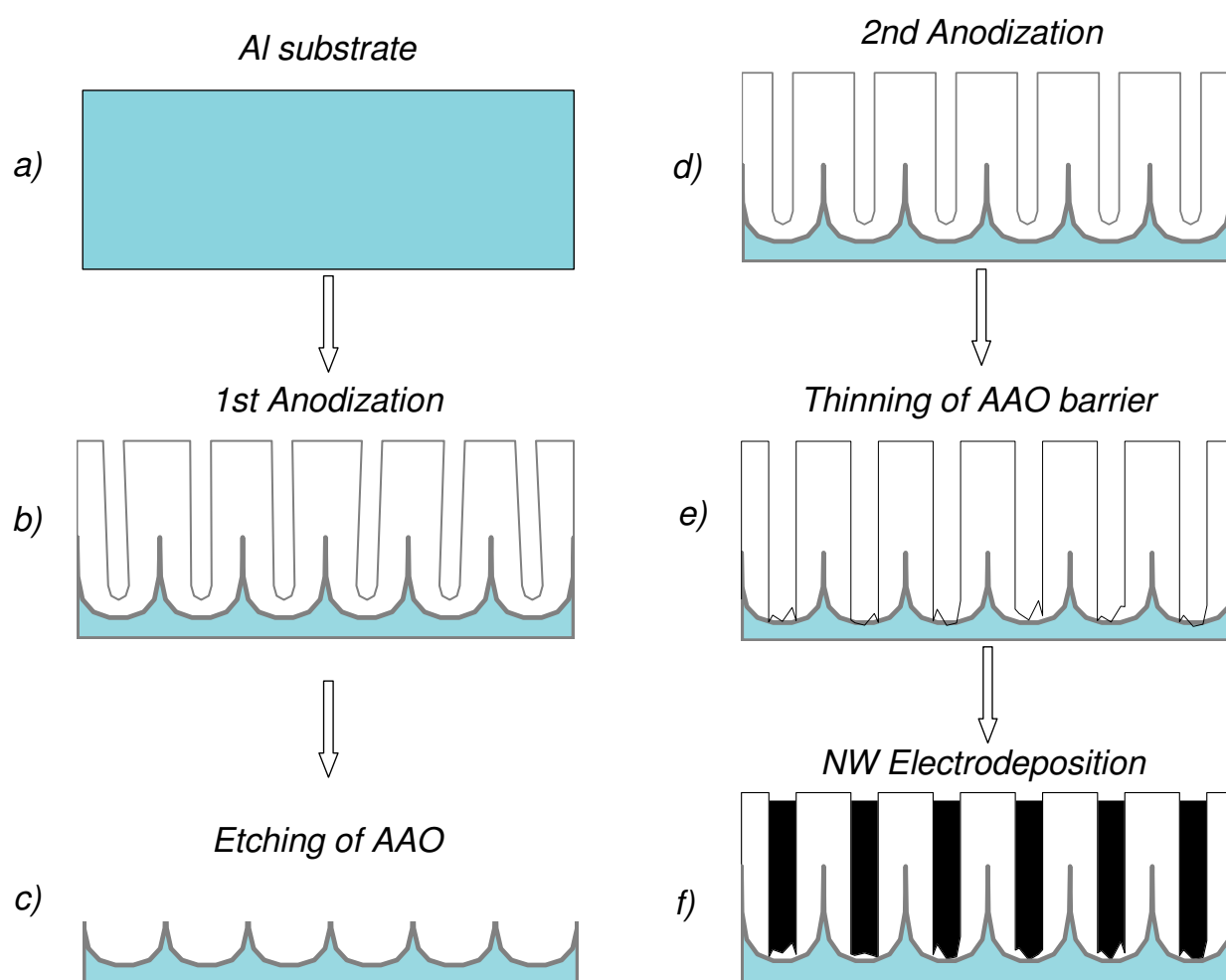

Fig. 1. Schematic representation of the Anodic Aluminum Oxide (AAO) template and the steps involved in the preparation of nanowires (after [Pirota *et al*, 2004]).

2.1 Structure

In Fig 2 we present the X-Ray diffraction scan of a Ni-electrodeposited NW array into a porous AAO membrane. We observe the crystalline Al peaks corresponding to the substrate and some broad and sharp peaks corresponding to the Ni NW. The nanoporous AAO

contributes to the broad background centred at $2\theta \sim 25^\circ$, indicating its amorphous structure. This AAO has not the structure or properties of the crystalline phases of Al_2O_3, such as the γ-Al_2O_3 or the high-temperature phase of α-Al_2O_3. Note that the Ni NWs are strongly textured along a generic [110] direction. This texture is also observed in NWs grown in AAO templates produced under sulphuric acid (with pore diameter $\phi \sim 20$nm) and oxalic acid ($\phi \sim 35$nm). We observed no preferential orientation for the AAO-template produced using phosphoric acid ($\phi \sim 180$nm) [Vassallo Brigneti 2009]. This possibly indicates a correlation of pore diameter with preferential orientation.
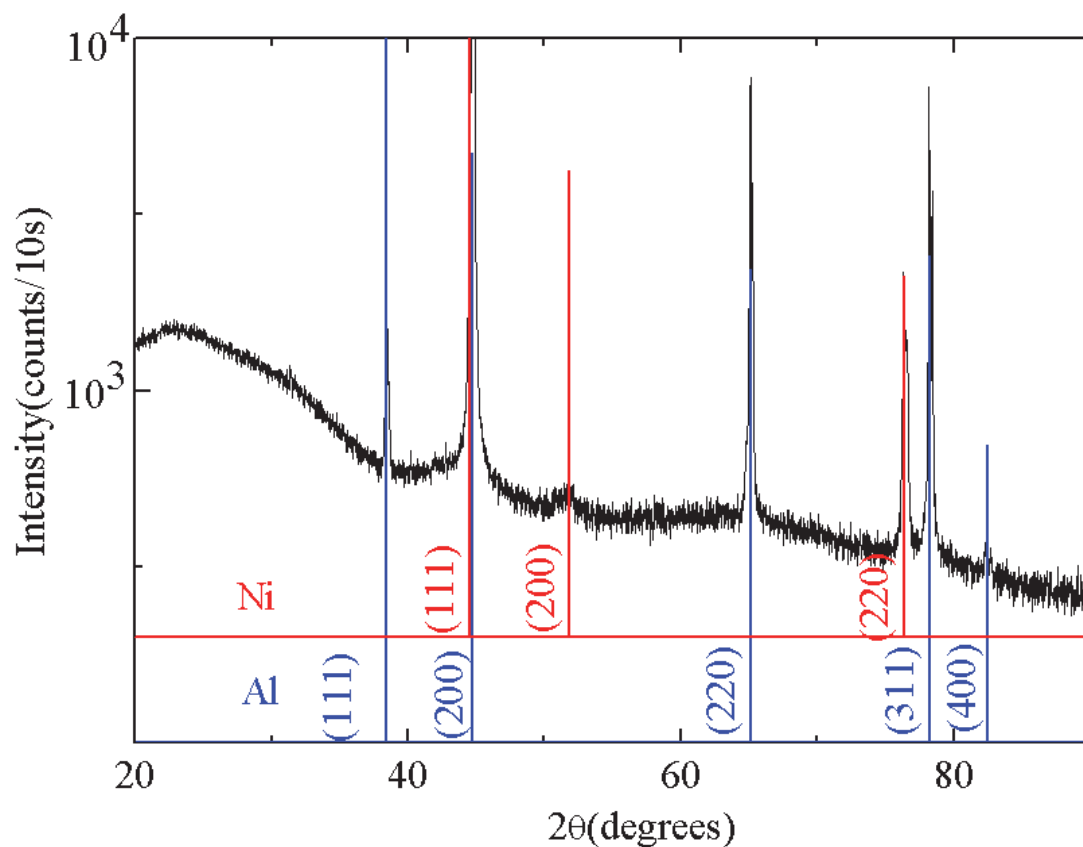

Fig. 2. XRD scan of a Ni NW array electroposited into an AAO membrane grown under oxalic acid. Most visible are the Al peaks from the substrate. The Ni NW grow with a <110> preferential orientation.

2.2 Surface microscopy characterization

In Figure 3 we show some of the SEM, AFM and MFM images of the samples used in this work. As mentioned previously, this figure shows that the AAO self organize into crystals of 1-2 μm^2 and the filling by the magnetic NW is almost perfect, to judged from the SEM image (top left) and MFM image (bottom right). Note the remarkable alignment of the AAO nanopores (up right) where a side view of the sample is presented. The detail of the AFM image (bottom left), as well as the SEM image, indicate some minor irregularities in the cylindrical shape of the NWs which is related with the hexagonal crystal deformation, as a

detailed study has shown [Vassallo Brigneti, 2009]. The MFM image, obtained in the remanent state after saturation (Fig 3a bottom right) shows the presence of some NWs clusters with reversed magnetization, seemingly due to the magnetic dipolar interaction between the wires (bright yellow in the image), yet most of the wires point on a preferential direction, which is consistent with the average magnetization in this system (see Fig. 4 below). The dark spots or clusters indicated the presence of NWs with reverse magnetization.
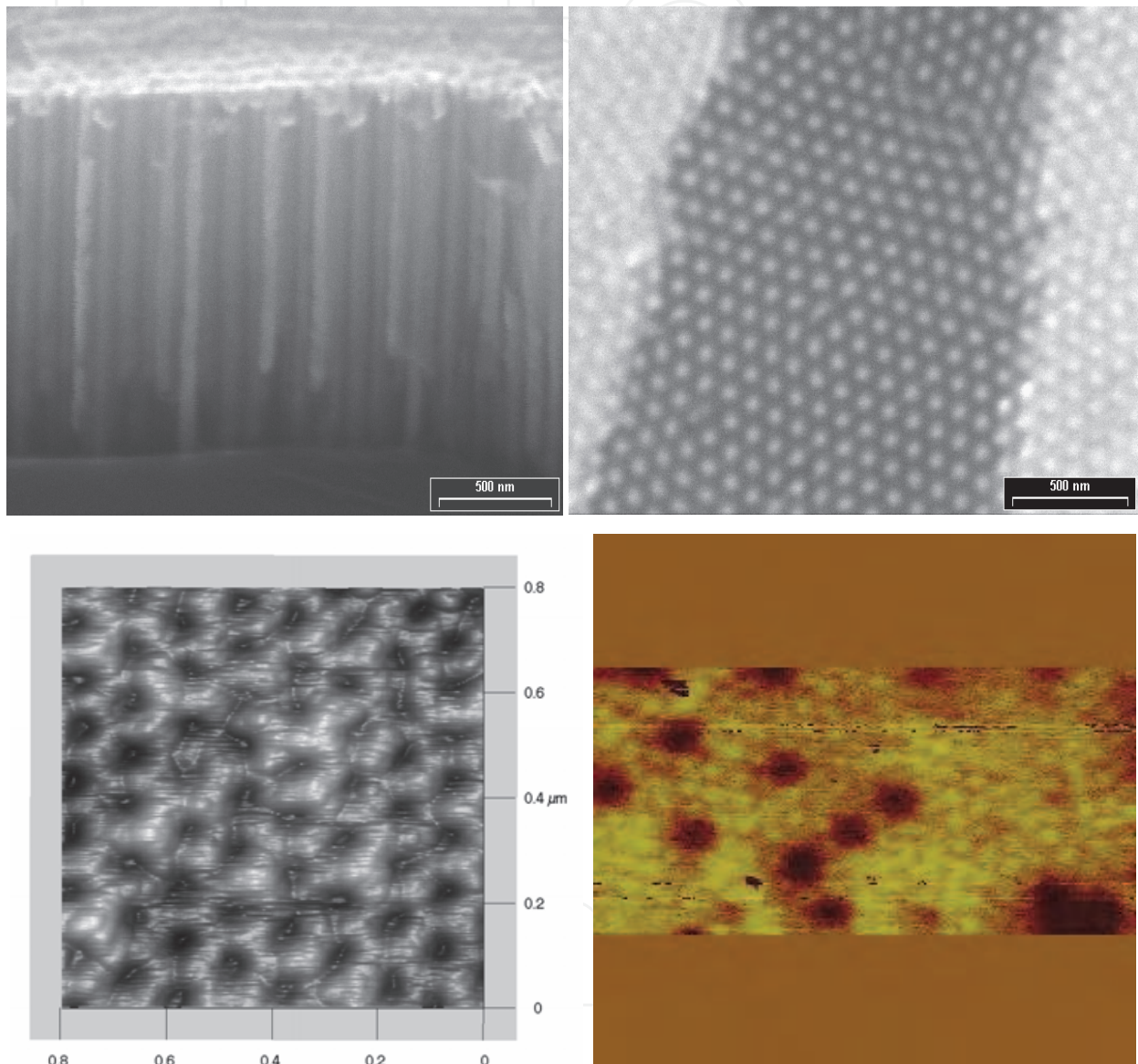

Fig. 3. (a) Top left : SEM top view of sample SNi. The clear dots are the Ni NWs. The hexagonal crystalline order extends through 1-2 µm^2. Top right: side view of the columnar shape of the AAO matrix Bottom left: AFM image Bottom right: (MFM) image performed on the remanent state after saturation (obtained with a Nanoscope IV). The dark spots correspond to inversely polarized NWs. Only a small portion of the wires display inversion. From images like these we estimate the NW diameter, $d \sim (37 \pm 4)$nm and inter-wire separation $S \sim (109 \pm 10)$ nm, derived from these quantities the filling factor of the NW is $f = (\pi/2\sqrt{3})\,(d/S)^2 = 0.106 \pm 0.015$.
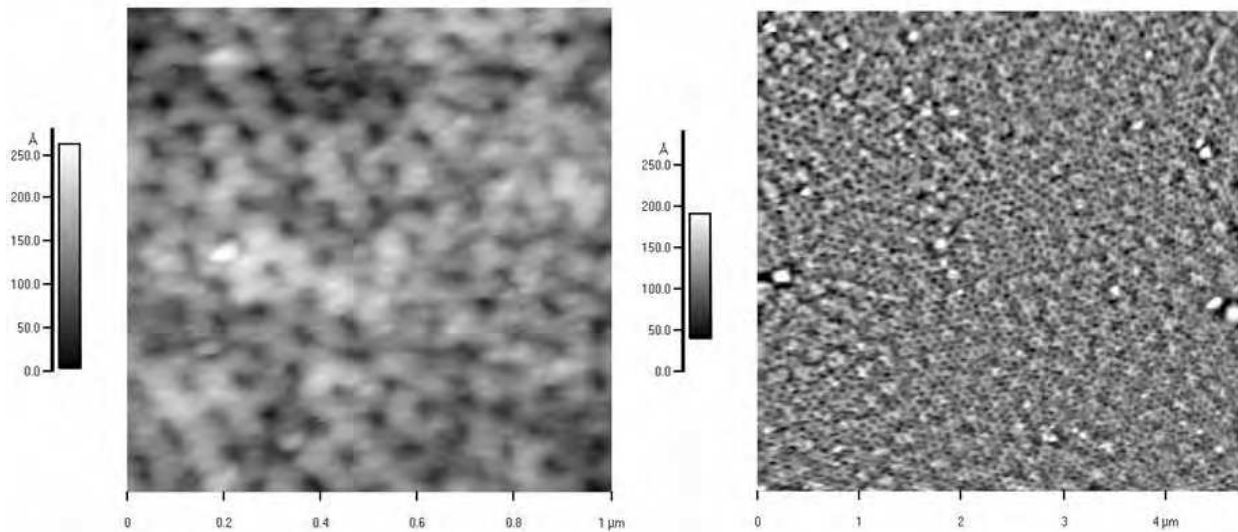
Fig. 3. (b) AFM scan of sample SA, fabricated under similar conditions but reducing the first anodization time to 3h instead of 72h (of sample SNi, Fig. 3a). Note that the hexagonal order is reduced and the disorder seems to increase as compared to sample SNi. From AFM images we estimate $d = (31 \pm 7)$nm and $S = (92 \pm 14)$nm, yielding $f = 0.103\pm0.03$.

2.3 Magnetic characterization by dc magnetization
The magnetization data was measured in a SQUID magnetometer and in a Lake Shore 7031 VSM.
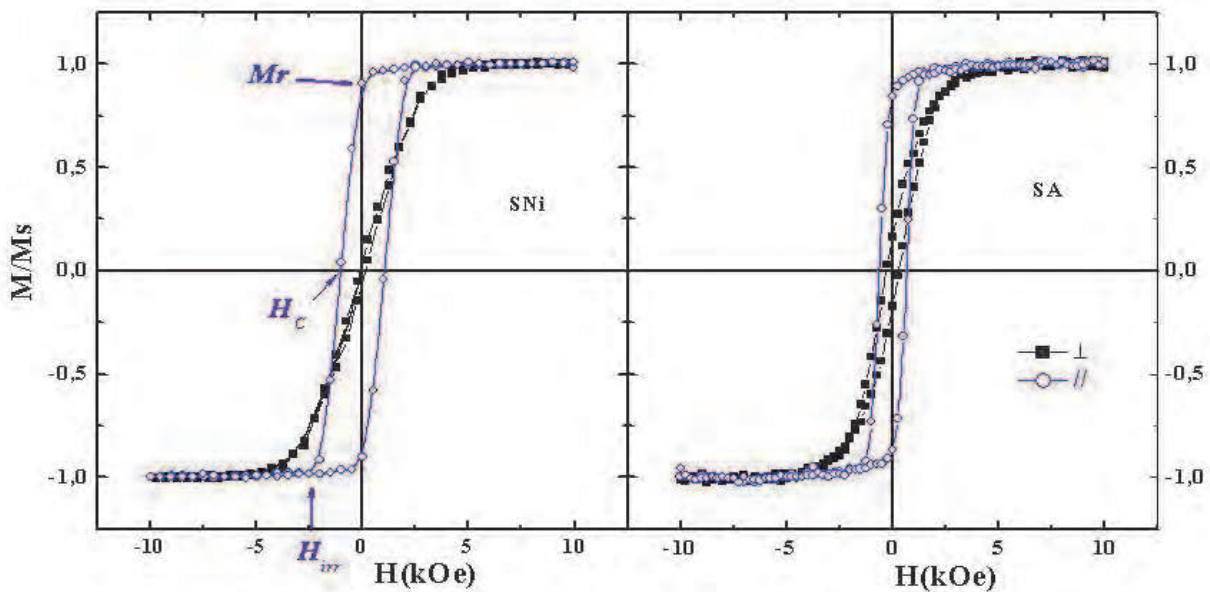

Fig. 4. Left: Magnetization of the Ni NW array under an applied field (sample SNi, Fig. 2 and 3) measured parallel (blue circles) and perpendicular (black squares) to the NW. The remanent magnetization (Mr), coercive (H_C), and irreversibility (H_{irr}) fields are indicated. Right: same for sample SA.

Fig. 4 shows hysteresis loops measured on samples SNi and SA. In Fig. 4 we indicate H_C, the irreversibility field, $Hirr$ (for $|H| > |Hirr|$ M is single-valued), and the remanent magnetization, Mr, which is close to 90% of saturation in these samples. This explains the large polarization observed in Fig. 3a by MFM after saturation. Ideally, in a uniaxial anisotropy system, the magnetization measured perpendicular to the easy axis should follow a linear behavior up to the saturation field, and this field should coincide with the anisotropy field, H_A. Observing Fig. 4 we notice that even though M($H \perp$NW) follows an almost-linear behavior at low H, it departs significantly from this behavior at larger fields making it difficult to define a unique value for H_A from M(H $\perp$). One of the interpretations of this effect resides on the fact that NWs, even though they can be well approximated as single-domains, do not behave internally as perfectly uniformly magnetized.

The departure from an ideal Stoner-Wohlfarth model [Brown, 1963] is due to the fact that the NWs can reverse the magnetization by inducing nucleating a vortex intermediate state or a transverse magnetization mechanism that implies a non-uniform reversal [Allende *et al.*, 2008; Hertel & Kirschner, 2004]. These mechanisms reduces the energy barrier which translates into a smaller H_C from what would be the uniform-reversal value ($H_C = H_A$). Yet, in the saturated state it is possible to define an average anisotropy field, H_A. In this sense FMR is very helpful as it measures directly H_A. The anisotropy field determined using FMR for this sample [see below] is H_A = 2.0(2) kOe, double than the coercive field, H_C. In sample SA the measured H_A is also significantly larger than the coercive field.

2.4 Magnetic resonance setup

The experiments were carried out in a Bruker ESP300 spectrometer at room temperature. As usual we use field modulation (10Oe-100kHz) to obtain the absorption derivative spectrum. The microwave field is perpendicular to the NW. We will present data on the bands operating at 1.2, 9.4 and 34 GHz, commonly known as L, X and Q-bands.

3. Ferromagnetic resonance and blocking in nanomagnetism

For over a decade there has been a growing interest in microwave response of magnetic NWs, stemming from basic and applied research [Boucher *et al.*, 2010; Darques *et al.*, 2009; Fert & Piraux, 1999]. One of the characteristic experiments in the microwave region (1-50GHz) is to study these nanostructured materials under a simultaneous presence of a uniform applied field, H, and an exciting microwave field usually applied perpendicular to H. The uniform field determines the natural precession frequency of the magnetization around the effective field which depends on: H, contributions due to shape anisotropy, dipolar interactions, crystal field, and magnetoelastic interactions. Ferromagnetic resonance (FMR) occurs when the microwave frequency matches the natural frequency of the magnetic system [Kittel, 2005]. The parameters that characterize a ferromagnetic system can be studied by measuring the power absorbed as a function of the microwave frequency and applied field, H. With the advent of vector analyzers (VNA) and microstrip exciting techniques microwave absorption can be studied conducted varying the frequency under a given H, or -as in the traditional FMR experiments- performed under a fixed frequency while sweeping H.

In apparent analogy with the FMR microwave absorption of nanoparticle systems stands the magnetic ac-susceptibility, χ_{ac}, usually measured under H = 0. This technique has

been extensively used to study non-interacting nanoparticles [Dorman *et al.*, 1997], spin-glass [Lundgren *et al.*, 1983; Mydosh, 1993], and random-field [King *et al.*, 1986; Ramos *et al.*, 1988] systems as it yields information on the system dynamics. Perfoming χ_{ac} as a function of temperature, *T*, in magnetic nanoparticle systems it is found that below a certain *T* the system is not able to respond to the alternating field, it is said that it "blocks". This blocking temperature, T_B, depends logarithmically with the exciting frequency [Dorman *et al*, 1997]. Yet, a *crucial* difference between χ_{ac} and FMR is that the first technique is usually carried out at *H* = 0 while FMR is not. The implications of this decisive difference have been overlooked and lead some authors to the conclusion that "blocking" occurs in FMR [Antoniak *et al.*, 2005; Berger *et al.*, 2001; Lubitz *et al.*, 2004; Sánchez *et al.*, 1999; Trunova *et al.*, 2009]. All these articles, dealing with magnetic nanoparticles, show that the ferromagnetic line broadens and its intensity decreases at low *T*, similarly to what is observed in χ_{ac} for T < T_B. Below we present data supporting the idea that the loss of FMR intensity observed is consistent with an effective anisotropy increase as *T* is lowered, and that there is no evidence of blocking in FMR in the sense of the χ_{ac}. We further explore the FMR response in the field region of magnetic hysteresis using one of the simplest nanomagnetic systems: single-domain magnetic NWs studied at three different exciting frequencies (1.2, 9.4 and 34.0 GHz) and as a function of the magnetic history of the sample.

3.1 Blocking in magnetic susceptibility

Magnetic systems possessing nearly degenerated energy minima are characterized by an extremely slow dynamics at low temperatures. This is evidenced in dc and ac susceptibility studies. Dispersed magnetic nanoparticles are among the simplest systems to study magnetic relaxation. Indeed, in these systems the magnetic relaxation depends on the anisotropy barrier, E_B, separating the two minima. For uniaxial anisotropy and zero applied field E_B = *KV*, where *K* is the uniaxial anisotropy energy per unit volume and *V* the particle volume. The characteristic time, τ, a particle will take to flip its magnetic state from one minimum to the other will depend on this energy barrier and the thermal energy and is given by [Dorman *et al.*, 1997]:

$$\tau = \tau_0 \exp\left(\frac{E_B}{kT}\right) \qquad (1)$$

where $1/\tau_0 \approx 10^9$ s^{-1} corresponds to a typical attempt frequency for reversal, *k* is the Boltzmann constant and *T* the temperature. As τ increases with decreasing *T*, for a given measuring time, τ_m, there will be a temperature, T_B, at which the magnetic moment is no longer able to fluctuate between the two minima and will, therefore remain in one of them. This temperature, T_B, is called the "blocking temperature". For a typical dc magnetization experiment $\tau_m \approx 100$s, and from Eq.(1) it follow the estimation $25kT_B \approx KV$ that relates the zero-field anisotropy energy barrier with T_B.

Magnetization measurements as a function of temperature, *M(T)*, are performed under a small dc field. This procedure leads to clear differences of the magnetic moment measured below T_B depending on whether the sample is cooled below T_B under zero field (ZFC) or under a field-cooled (FC) condition, using in both cases the same small dc field for measuring. In ideal uniaxial-anisotropy nanoparticle systems the ZFC is characterized by a

much smaller magnetization at $T \ll T_B$ than the corresponding FC state, up to $T \approx T_B$ [De Biasi *et al*, 2008]. T_B depends on the magnitude of H and $T_B(H) \to 0$ when the Zeeman energy equals the anisotropy barrier. For $T < T_B$ these systems behave as ferromagnets and present magnetic hysteresis in the $M(H)$ cycles. The maximum field for which the two branches merge defines the irreversibility field, H_{irr}, above which the system reaches an unambiguous magnetic state (see Figure 4).

3.2 FMR dispersion relation

In traditional FMR experiments the dc field is swept while keeping a constant microwave exciting frequency. While the field is swept the eigenfrequency of the system varies according to the Smit and Beljers dispersion relation [Smit & Beljers 1955, Morrish, 2001]:

$$\left(\frac{\omega}{\gamma}\right)^2 = \frac{\left(E_{\theta\theta}E_{\varphi\varphi} - E_{\theta\varphi}^2\right)}{(M_S \sin\theta)^2}\Bigg|_{\theta=\theta_0, \varphi=\varphi_0} \tag{2}$$

where $\omega = 2\pi\nu$, ν being the microwave frequency, $\gamma = g\mu_B/\hbar$ is the gyromagnetic factor, M_S is the saturation magnetization, $E_{\theta\theta}$, $E_{\varphi\varphi}$, and $E_{\theta\varphi}$ are the second derivatives of the free energy (E) with respect to the spherical angles (θ, φ) evaluated at the magnetization equilibrium direction (θ_0, φ_0), which is obtained from the free energy setting the first derivatives to zero ($E_\theta = 0$ and $E_\varphi = 0$).

This eigenfrequency reduces to:

$$\omega = (\gamma / M_s)\sqrt{E_{\theta\theta}E_{\varphi\varphi}} \tag{3}$$

evaluated at the equilibrium positions for the cases considered in this work. Eq (3) indicates that eigenfrequency is proportional to the geometric mean of the energy curvature along two perpendicular directions: θ and φ. We hope to clarify this concept in the simplified model developed in the next sub-section.

3.3 Uniaxial anisotropy model

In order to show how the sample's magnetic history affects the FMR, and compare this situation with the magnetic hysteresis cycle, we consider here a *uniformly magnetized system* with second order uniaxial anisotropy described by the free energy per unit volume, E:

$$E = -M_S H \sin\theta \cos(\varphi - \varphi_H) - K \sin^2\theta \cos^2\varphi \tag{4}$$

where H is the external magnetic field applied in the X-Y plane, M_S and K are the magnetization and anisotropy energy per unit volume, φ is the magnetization angle away from the easy axis (considered parallel the X-axis) and φ_H is the angle H makes with the X axis. This particular arrangement, represented in figure 5, describes a general case of a uniaxial magnetic anisotropy under an applied field and has the advantage of being mathematically simpler (solving $E_\theta = 0$, yields $\theta_0 = \pi/2$ in Eq. (2) as the magnetization equilibrium orientation).
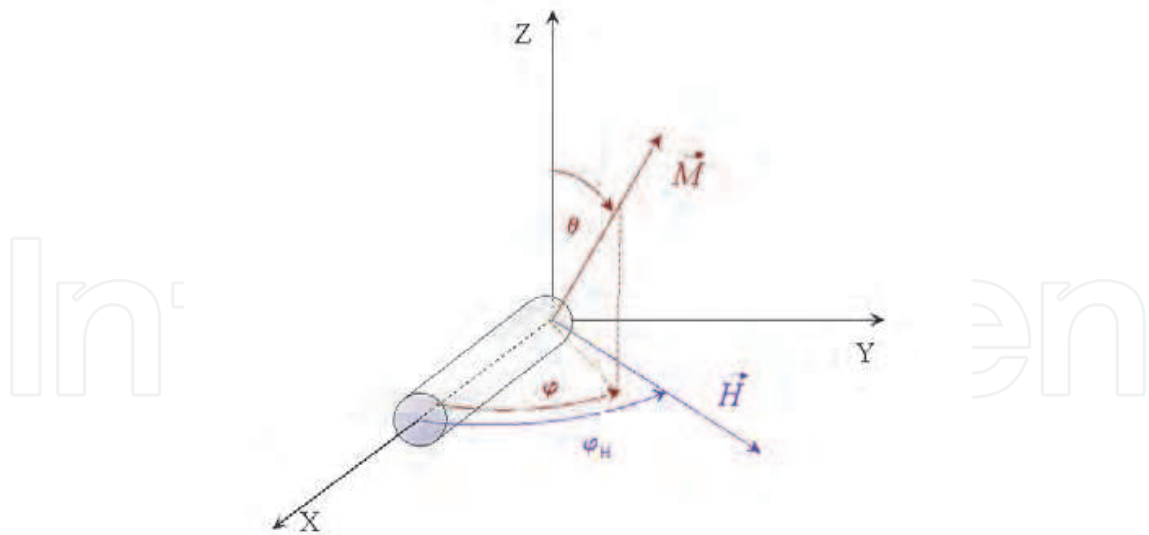
Fig. 5. Reference frame in which the NW axis coincides with the X direction. The magnetic field moves in the X-Y plane.

We will consider the application of H parallel or antiparallel to the anisotropy axis ($\varphi_H = 0$, π). In this way the magnetic system can be in either one of two states for $H < H_A$ ($H_A = 2K/M_S$). In this simplified model the coercive field, $H_C = H_A$.
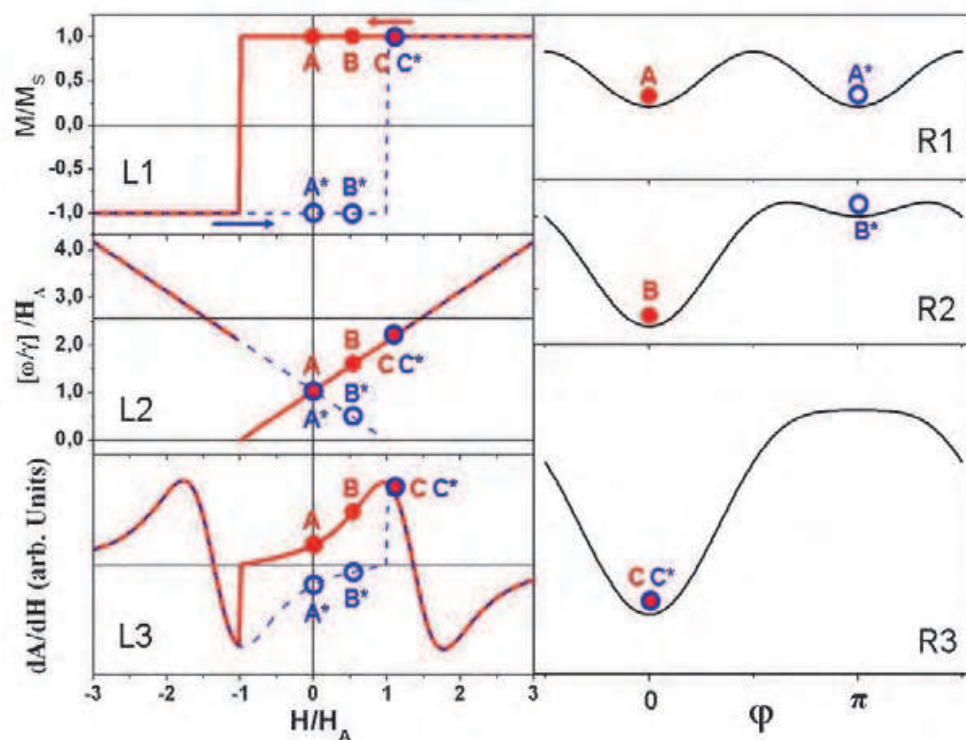

Fig. 6. R1-R3 energy landscape as a function of φ for $\varphi_H = 0$ (Eq. 4). L1 hysterisis cycle. L2 dispersion relation (Eq. 3). In panel L3 we show the calculated absorption derivative for the conditions: initial magnetization pointing along the applied field (A$\rightarrow$ B$\rightarrow$ C) in solid red line, and initial magnetization in the opposite sense (A*$\rightarrow$ B*$\rightarrow$ C*) in blue dash line.

In Figure 6 we represent the *M(H)* hysteresis loop (L1). Decreasing *H* from saturation (C→ B→ A) the magnetization will remain saturated in the positive direction down to the field -*H* = H_A, at which point it will reverse for -*H* > H_A (full red line). Similarly, increasing *H* from saturation in the negative direction (dashed blue curve) the magnetic state will follow the points A*, B* and C*. On the right panels R1-R3 we have plot the energy landscapes as a function of the magnetization direction, φ, for three different fields, *H/ H_A* = 0, 0.5 and 1.1 applied along the easy axis, corresponding to the points A, B, and C. For zero applied field the energy minima at φ = 0 and φ = π are equivalent (Figure 5 - R1). The sequence R1-R2-R3 follows the points A-B-C of the hysteresis loop for the field applied along the easy axis. Looking at the sequence R1→ R2→ R3 we see that the curvature, given by $E_{φφ}$, increases for the equilibrium condition at φ = 0 for increasing *H*. If the magnetization was initially opposite to *H* (points A*, B*), the energy curvature calculated at φ = π will *decrease* with increasing *H* up to the point at which there will be a single minimum, at *H* = H_A. Directly related with the energy curvature is the dispersion relation, drawn in Fig. 6 (L2) as full (red) and dash (blue) lines. The horizontal line in L2 corresponds to the microwave frequency, fixed in the traditional FMR experiment. The point at which the dispersion relation crosses this microwave frequency is the resonance field, H_R. Panel L3 shows the calculated microwave absorption derivative. To simulate the FMR spectra we used Netzelmann`s equations [Netzelmann, 1990] with g = 2 and α = 0.3. Note that in Eq. 3 we have two possible equilibrium positions within the hysteresis cycle. Both equilibrium positions are, indeed, possible states. As shown in L2 when the magnetization is in the same sense as the applied field, the dispersion relation grows (full red line) with *H*, reaching the resonance condition at $H_R = ω/γ$ - H_A (for ω/γ > H_A). If, on the contrary, the sample is initially oppositely magnetized (A*) and the field is increased the dispersion relation *decreases* (following the curvature decrease observed in B*, see R2), thus going away from the resonance condition (dash blue line in L2). The result, in the absorption spectrum calculated in L3, is the observation of a "tail", as though the absorption occurred at negative fields. This "tail" would continue to decrease in increasing H up to the irreversibility field at *H* = H_A and would jump to the "normal" absorption (red solid line) at larger fields. Note that L3 indicates absorption occurs even at H = 0 within this simple model. This would be so as long as the exciting microwave frequency and the natural frequency are close to each other (measured in linewidths units).

In spite of the simplicity of the model it describes some of the most significant features observed. Only within the irreversibility region we could expect to see the effects of the sample magnetic history.

As shown in Figure 6-L2 there is a minimum frequency, ν = $γH_A/2π$, below which there will be no resonant microwave absorption, when *H* is applied near the parallel direction. This defines an anisotropy gap. If the anisotropy gap increases (as is found in superparamagnetic nanoparticle systems) we may expect, in some cases, to reach the condition in which H_A > ω/γ and therefore the resonance condition would be lost for the parallel condition and for all directions close to the easy axis. The consequence would be a sudden intensity drop. Yet this effect cannot be related to the blocking: if it were so then experiments at higher frequencies would not be able to yield absorption signals, which is not what has been found in experiments [Ennas *et al*., 1998].

Comparison of the measured magnetization loop along the easy axis (Fig. 4) with a Stoner-Wolhfarth hysteresis cycle of Fig. 6-L1 indicates that the total magnetization switches progressively. As observed in the magnetic state in Fig. 3 bottom right, these NWs are pointing either up or down, and the total magnetization is the result of the addition of all the NWs contribution. Thus, we can talk about the NW "population" at $\varphi = 0$ and $\varphi = \pi$. Then, a phenomenological way to reproduce the measured hysteresis cycle is to consider that these populations change as a continuous function of the applied field. For this purpose we used a hyperbolic tangent of the applied field (offset by H_C) and adjusted the transition width to best reproduce the experimental data. Having a function that describes correctly the hysteresis cycle we proceeded to model the FMR response based in the simple model outlined in this section with the basic ingredient that the population of each well (amount of magnetization pointing parallel or antiparallel to the applied field) is a function of the applied field, set to reproduce the hysteresis cycle. This is what we describe in sub-section 3.6 and compare with experiments.

3.4 FMR dispersion relation and angular variation in Ni NW arrays

Using the expression for the energy given by Eq. (4) and evaluating Eq. (2) at the equilibrium angles $\theta_0 = \pi/2$ and $\varphi = \varphi_0$ the following dispersion is obtained:

$$\left(\frac{\omega}{\gamma}\right)^2 = [H\cos(\varphi - \varphi_H) + H_A\cos^2\varphi][H\cos(\varphi - \varphi_H) + H_A\cos 2\varphi] \tag{5}$$

where $H_A = 2K/M_S$ is the anisotropy field. The observed angular variation at X band (9.4 GHz) of sample SNi is shown in Figure 7. The magnetic field that satisfies Eq. (5) is the resonant field.

For the particular conditions $H//$ and $\perp$ to the wires Eq. (5) adopts the expressions:

$$\frac{\omega}{\gamma} = H + H_A \tag{6}$$

for $H_A > 0$ and $H//$ easy axis

If H is applied with the magnetization pointing initially opposite then, for the limited region within the hysteresis cycle where the magnetization is reversed, Eq. 6 changes to $(\omega/\gamma) = H_A - H$ as discussed previously in relation to Fig. 6-L2.

For the particular condition $H\perp$ to the wires Eq. (5) adopt the following expressions:

$$\left(\frac{\omega}{\gamma}\right)^2 = (H_A^2 - H^2) \tag{7a}$$

for $H < H_A$ and $H \perp$ easy axis
and

$$\left(\frac{\omega}{\gamma}\right)^2 = H(H - H_A) \tag{7b}$$
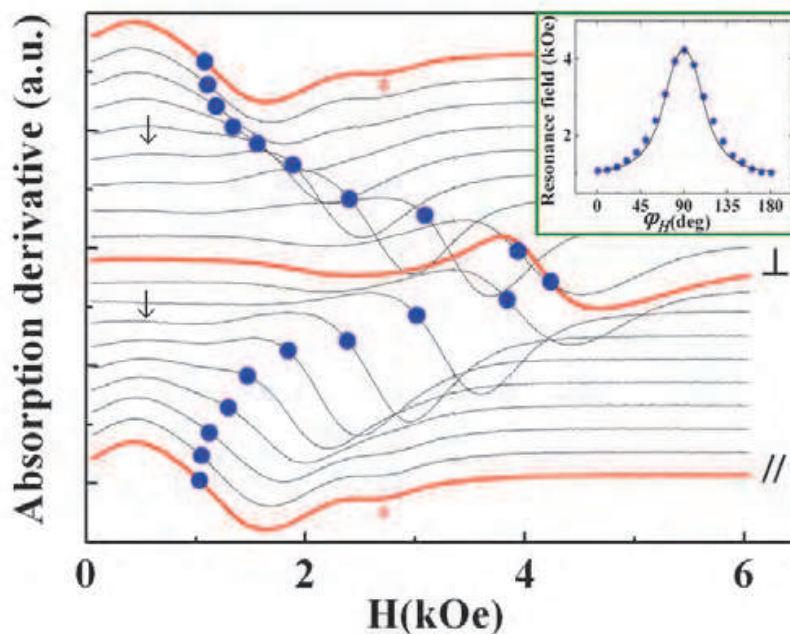
for $H > H_A > 0$ and $H \perp$ easy axis

Fig. 7. Angular variation of sample FMR spectra obtained at 9.4 GHz (X-Band). The directions // and ⊥ indicate the conditions for which the field is applied parallel and perpendicular to the wires, respectively. The dots indicate the resonance field. Upper right inset: resonance field as a function of the externally applied field angle, φ_H. The full line is a non-linear least-square fit to the experimental data.

Using a non-linear least-square routine to fit the phenomenological parameters of Eq(6) from the observed angular variation, we obtained the following values for this sample: H_A = 1.99 ± 0.08 kOe and g = 2.19± 0.04. The g-factor is consistent with the Ni bulk value g = (2.18-2.21) reported in the literature [Farle, 1998] and with previously reported values for Ni NWs [Ebels *et al.*, 2001; Ramos *et al.*, 2004a; 2004b]. Dipolar interactions among the wires decrease the effective anisotropy. Indeed, for the case of a homogeneous porous membrane filled with NWs, with filling factor *f*: $H_A \approx 2\pi M_S (1 - 3f)$, where M_S is the saturation magnetization per unit volume. In our case *f* = 0.106 ± 0.015 and for M_S = 485 G we obtain H_A = 2.1 ± 0.2 kOe, consistent with the measured value (an isolated single domain NW would be expected to have $H_A = 2\pi M_S$ = 3.0 kOe, thus dipolar interactions seem to account for the experimentally measured H_A).

Apart from this remarkable agreement there are some small features in the absorption derivative spectra that we consider now. In the main panel of Figure 7, signaled by "↓", we have indicated a low-field absorption which is more clearly observed away from the parallel direction. This low-field absorption distorts the main line, particularly at intermediate angles between the // and ⊥ directions, thus we did not use these points in the fit (the range of 40-70 degrees away from the easy axis). Li *et al.* [Li *et al.*, 2005] claim that head-on domains as the ones responsible for this low-field line, particularly in the H ⊥ NW condition. An alternative explanation for the broad absorption observed in this direction is that a "tail" of the dispersion relation given in Eq. 7b would be the origin for this low-field "line", particularly in the perpendicular direction (see Fig. 8). In Figure 9 we have drawn the dispersion relation for several angles, and particularly the dispersion relation given by Eq. 7b and 7a using the parameters measured for this sample. In order to test the hypothesis of a non-resonant contribution to the absorption that could come from the Eq. 7b, we have plot in Figure 9 the

calculated effect on the FMR spectrum for $H < H_A$ (Eq. 7b) and for $H > H_A$ (Eq. 7a) and compare this calculation with the experimental data. The agreement is remarkable despite the fact that the dispersion relation, does not soften down to $\omega = 0$ [Encinas-Oropesa et al., 2001]. The fact that the dispersion relation does not soften down to reach $\omega = 0$ in the hard direction may be connected to the shortcomings of describing all the magnetic spins in a NW as performing a uniform precession characterized by a single uniaxial anisotropy.

Another feature, indicated with an asterisk in the FMR spectra of Figure 7, is pointing to an absorption occurring at fields higher than the main resonance in the condition H//NWs. We speculate this absorption may be due to a mode localized near the NW ends. If so the intensity of this absorption should decrease with increasing NW length. While this is not apparent in the data of [Ramos *et al.*, 2004a], it turns out that this higher-field absorption decays, in comparison with the main line, as 1/L, where L is the NW length.

As mentioned previously maximum power absorption occurs when the eigen-frequency matches the exciting microwave frequency at the resonance condition (Fig. 8). This condition is met at $H = H_R$, the resonance field. As long as $H_R > H_{irr}$, the resonance spectrum does not depend on the magnetic sample history. In magnetic NW arrays in the region $H < H_{irr}$ the microwave absorption may depend on the magnetic history [Ramos *et al.*, 2007; De la Torre Medina *et al.*, 2010] as explained in the previous subsection.
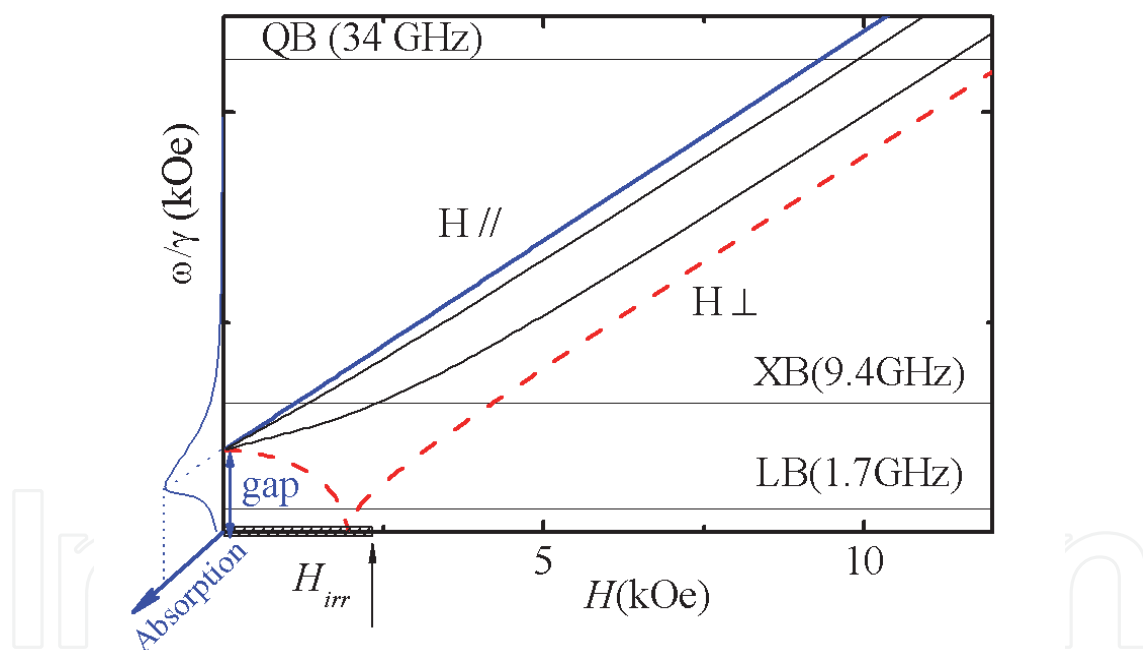

Fig. 8. Dispersion relation ω/γ vs H of an ideal uniaxial ferromagnet, for $H//$ easy-axis (straight blue line - Eq 6) and $H\perp$ easy-axis (dashed red line, Eq. 7a,b). Two additional dispersion relations corresponding to H applied at 30 and 60 degrees off the easy axis are drawn as full black lines. The $\omega/\gamma = H_A$ gap, at $H = 0$, is indicated by a vertical double-tip arrow. For $H//$ easy-axis the resonance condition for 9.4 GHz (X-Band) is reached below the irreversibility field, H_{irr} (see Fig. 4). The ω/γ corresponding to 1.2 GHz (L-Band), 9.4 GHz (X-Band) and 34 GHz (Q-Band) and g = 2.2 are indicated as horizontal lines. We have also drawn a schematic Lorentzian line centered at the gap, corresponding to the absorption as a function of frequency for $H = 0$. This absorption profile was drawn considering a third axis coming out of the paper.

In Figure 8 we have marked a hysteretic region covering $|H| < H_{irr}$ = 2.2kOe, indicated as a hatched rectangle on H-axis. Below H_{irr} a hysteretic behavior is observed in the magnetization data and in the FMR spectra LB and XB *only*. Changing the exciting frequency (L, X or Q band) we may choose situations in which the exciting frequency is below the gap (L-band), near the gap (X-band) and above it (Q-band).

A Lorentzian absorption profile is drawn in Fig. 8 centered at H = 0, the intensity of this Lorentzian is schematically shown as a third axis. For a fixed H as function of ω/γ we expect to find an absorption similar to this shape, the position of the maximum changes with H following closely the dispersion relation, as has been experimentally observed [Encinas-Oropesa *et al*, 2001]. We observed absorption at H = 0 at L-Band and at X-Bands as the line-width superimposes with the exciting frequency.

To simulate the FMR spectra in the case $H\perp$ NW we consider a Lorentzian absorption centered at a field given by the dispersion relation. The field at which the dispersion relation reaches its minimum ($H = H_A$) corresponds to the minimum of the absorption derivative. This simple model (Fig. 9: blue dash-line) follows well the observed experimental results (blue solid line). For simulating the $H//$ NW spectrum we considered a low-intensity additional line centered near 2.5kOe, and the fact that a small portion of the NW are inverted near H = 0, as indicated by the remanent magnetization being 90% of its full value. This partial non-saturation explains, at least partially, the observation of a low-field peak (0.4 kOe) smaller than the high-field (1.6kOe) peak. We will return to the the simulation within the irreversibility region in 3.6.
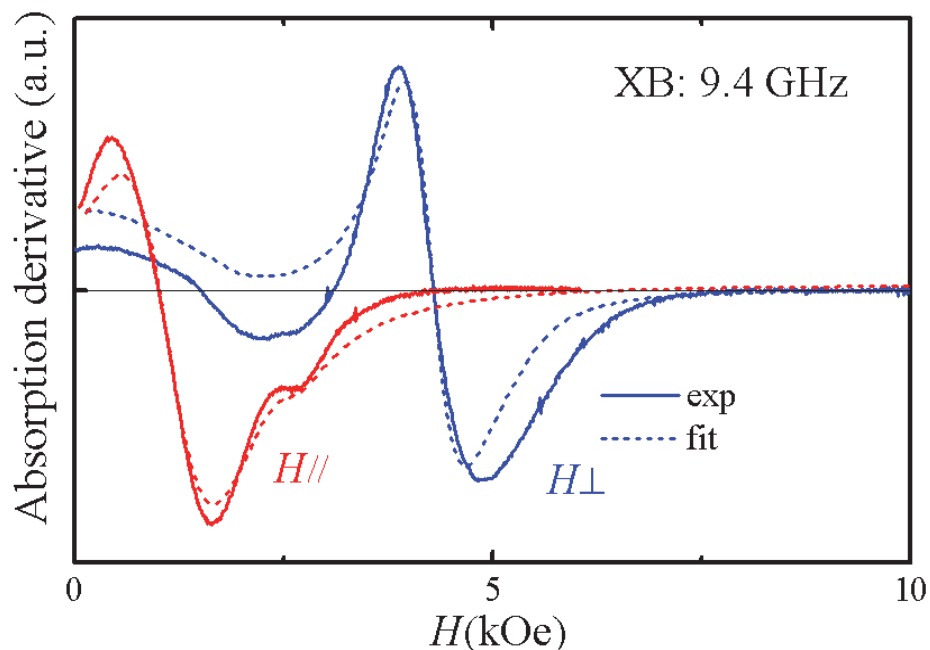

Fig. 9. FMR spectra of sample SNi (9.4 GHz) for $H//$ and $H \perp$ to the NWs. The main line position is well described by a single anisotropy field (Eq. 6 and 7). The dash lines are fits considering the dispersion relation with a suitable width. In both cases the zero-field absorption is well reproduced by this simple model.

Many of these low-field effects associated to the proximity of the anisotropy gap disappear when the sample is studied at higher frequencies. We show results of the data obtained at

34.0GHz on the two samples SNi and SA One of the difference between SNi and SA is its local order, which in greater in sample SNi. In Fig 10 we show the measured angular variation and peak-to-peak line-width, ΔH_{pp}.
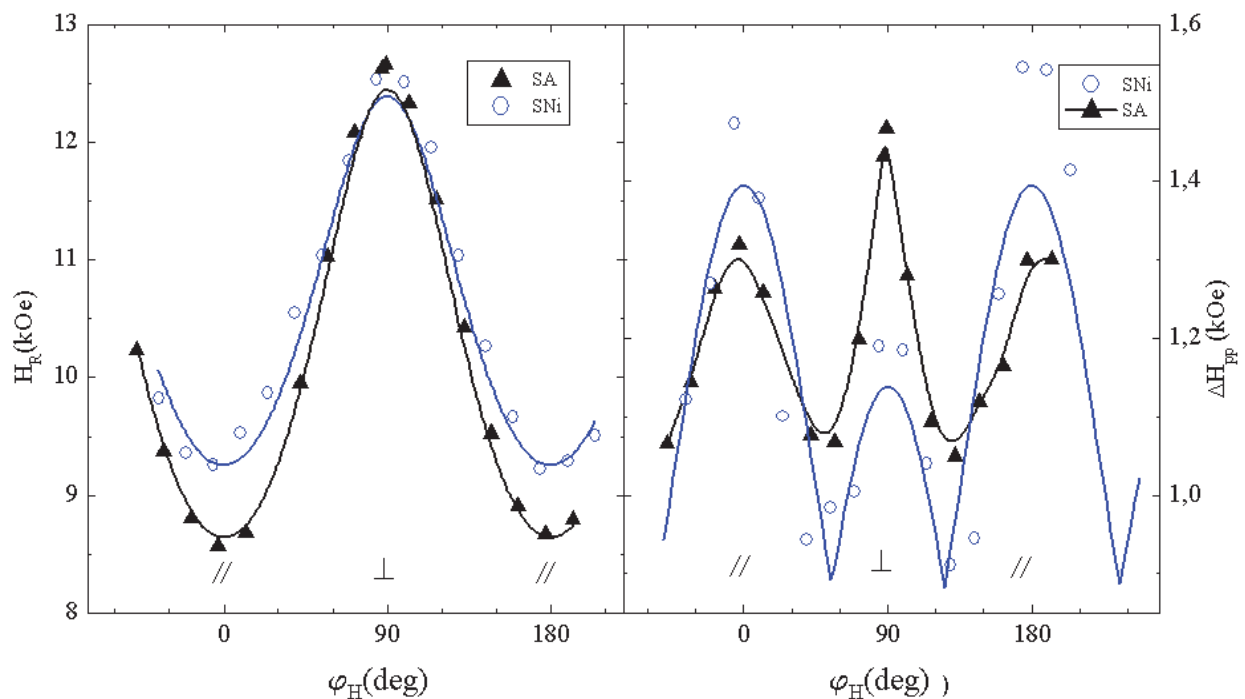

Fig. 10. Left: observed angular variation of the FMR spectra obtained at 34.0 GHz, for the samples reported. Right: observed angular variation of the line-width. This ΔHpp for SNi was fit to a model including variation of f and the NW angle orientation (blue line) The B-Spline fit to the data of SA is shown as a solid black line.

The fits of Eq. 5 to the data shown in the left panel of Fig. 10 yield g = (2.16 ± 0.03) and (2.20 ± 0.02) for sample SNi and SA respectively, and the effective anisotropy fields H_A = (2.1 ± 0.2) kOe and (2.49 ± 0.08) kOe for SNi and SA respectively. The g-value is consistent with the reported values for Ni. The larger value for the anisotropy field in sample SA may be related with a smaller filling factor suggested by the AFM images.

As these NWs have aspect ratios ~30 and ~80 for sample SA and SNi respectively, the self-demagnetizing factor along the wire length is negligible. The observed departure from the isolated value $H_A = 2\pi Ms$ = 3.08kOe can be attributed to dipolar interactions, as has been clearly established previously [Ebels *et al.*, 2001; Encinas-Oropesa e*t al.*, 2001; Ramos *et al.*, 2004a; 2004b]. There is no indication of tension along the wires, as characterized by X-Ray diffraction in Figure 2 [Vassallo Brigneti, 2009]. Even though the NW grow textured along the [110] direction the crystal field is small (~ 0,2 kOe), which cannot explain the relatively large linewidths observed in Fig 10 right panel. Ebels *et al.* suggest a Gilbert-damping contribution to ΔH_{pp} ~ 0.4 kOe independent of angle should be present. Other sources of line broadening can come from variations in the filling factor, f, and from NW misalignment with the AAO surface. This last option, however, can be discarded. Indeed, NW misalignment would produce a *maximum* at the angle of maximum variation of the resonance field with φ_H. We performed a least square fit using a model that takes into account variations in Δf, as well as the NW angular deviation to ΔH_{pp} and we obtained, for sample SNi: $\Delta f/f$ = (18 ± 6) %, an

angular dispersion of (0 ± 3)deg, and a base-line-width of 0.87kOe. The blue line with sharp minima on the right corresponds to this fit [Vassallo Brigneti, 2009]. A similar discussion regarding this type of fit was also considered by Ebels et al, 2001.

A simple calculation indicates that the demagnetizing field when the sample is polarized along the NW, depends on the average filling factor, f, and not on the "local" disorder [Vassallo Brineti, 2009]. More difficult to explain with variations in f alone is the absolute maximum observed in ΔH_{pp} of sample SA in the condition $H \perp$ NW. Previously we considered geometrical local disorder as the main cause for this increased linewidth observed in the perpendicular direction [Vázquez et al., 2005]. More recently we have realized that consideration of local deformations from the ideal cylindrical shape of the NWs is very effective in producing large variations of the resonance field in the perpendicular direction, much more than in the parallel direction [Vassallo Brigneti,2009]. This correlates the obseved maximum at $H \perp$NW with the larger lattice disorder [Vassallo Brigneti 2009].

3.5 Consequences on the FMR applied to nanoparticles

In non-interacting superparamagnetic nanoparticle systems magnetization follows a (H/T)-scaling behavior. Thermal fluctuations decrease the effective uniaxial anisotropy field, H_{Aeff}. This H_{Aeff} increases as the T is reduced while preserving the uniaxial symmetry [De Biasi et al., 2003; Dorman et al., 1997; Pujada et al., 2003; Raikher & Stepanov, 1994]. If we consider an initial anisotropy gap smaller than the exciting frequency (as in Figure 8 for X-Band and the gap shown), we may expect an increase of the effective anisotropy field as T is lowered [De Biasi et al., 2003; Raikher& Stepanov, 1994] and the condition of a gap larger than ω/γ is likely to be reached. As the anisotropy gap exceeds the microwave frequency the nanoparticles whose easy axes are close to the direction of the applied field will not longer reach the resonance condition. We concluded this is what happens in some nanoparticles at low temperature [DeBiasi et al., 2004; 2005] that evidence an intensity drop as the effective anisotropy field becomes greater than ω/γ. In previous works [Antoniak et al., 2005; Berger et al., 2001; Sánchez et al., 1999] this intensity loss was associated with "blocking" in the sense that the magnetic system was not able to follow the microwave excitation frequency $\nu \approx 10^{10}$ GHz (X band) below this "blocking" temperature. If that would be the case then, at the same temperature, the system would not be able to show any sign of resonance at a *higher* frequency, such as Q-band (35GHz), which is not the case (see also, [Ennas et al, 1998]). In this work we use this ideal "blocked" Ni NWs to study the system at three different frequencies and as a function of the sample history.

In spite of the apparent restrictive case of ferromagnetic NW we want to emphasize that the consequences on the *line-shape* and resonance condition of other ferromagnets with large uniaxial anisotropy is straight forward [De Biasi et al., 2003; Winkler et al., 2004]. In these cases the FMR spectra could be satisfactorily accounted for as a collection of randomly-oriented uniaxial ferromagnets. This line-shape can be readily distinguished from paramagnetic phases [Winkler et al., 2007; Likodimos & Pissas, 2007; Tovar et al., 2008] that coexist in the material, such the case of mixed-valence manganites. Indeed, this phase coexistence seems to be the cause of the large magnetoresistance effects observed in these colossal-magneto-resistance materials (CMR).

3.6 FMR results in the irreversible region

In this section we present FMR results on sample SNi, characterized in Fig 1- 4. The sample under study is made up of individual NWs subject to its own shape anisotropy, and dipolar

interactions among them. This sample is constituted of NW which can be approximated as single domain uniaxial ferromagnets which are "blocked" -in the sense of magnetic nanoparticles- and have the virtue of being aligned along the NW direction.

Two spectra types are shown in Figure 11: one in which the sample initial magnetization is polarized in the same direction as the field sweep (*H// * Mi, blue circles in Fig. 11, which we will call DP, for direct polarization), and a second experiment (*H// *-Mi, red triangles in Fig. 11, referred to as RP for reverse polarization) in which the sample is initially polarized in the reverse direction of the field sweep.
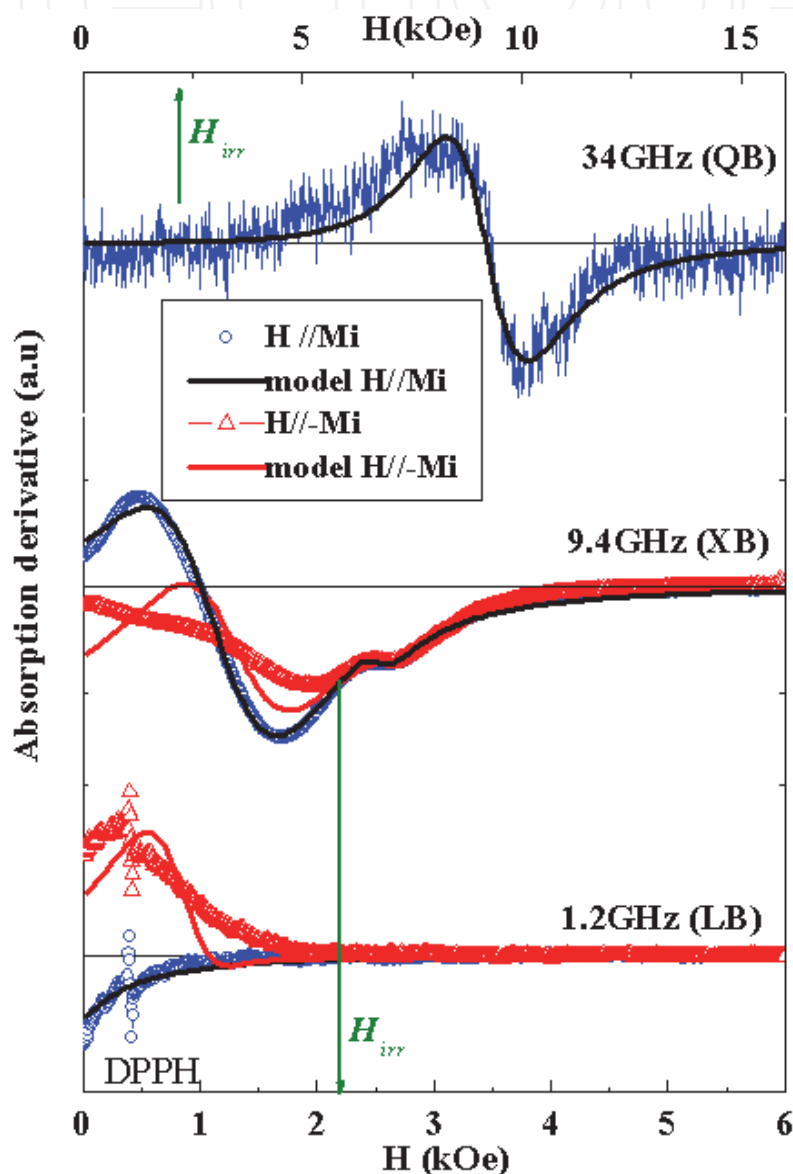

Fig. 11. FMR for sample SNi measured at three different frequencies, 34.0, 9.4 and 1.2 GHz, corresponding to Q, X and L-bands respectively. All data was obtained at room temperature in the condition *H//* NW after saturation in the same direction, and therefore the remanent magnetization is in the same direction as the field (*H//* Mi, blue circles) and the reverse initial magnetization (*H//*-Mi, open red triangles). The black (and red) full lines correspond to the model detailed in the text.

The RP was obtained using a compensating coil and reducing the field after saturation to (0.0 ± 0.1) Oe, as measured by the Hall sensor that regulates *H*. Afterwards the sample was rotated by 180 degrees while the magnet was kept at *H* = 0 and then the condition RP could be achieved. No significant changes where observed between DP and RP at 34GHz, particularly below *Hirr*, therefore we only plot the DP spectrum. A significant difference between DP and RP is observed below *Hirr* at 9.4 and 1.2 GHz,. At H = *Hirr* DP and RP merge into a single signal. More remarkably, the signal is initially positive in the condition *H//*Mi at X band and *negative* under the same condition in L-Band. Particularly at L-Band it is very helpful to record simultaneously a DPPH g–marker, as it indicates the field and is an intrinsic calibration of the instrument *phase*, therefore indicates clearly that the initial signal is negative. The full lines correspond to a fit of the model described in association with Figure 6. The model consists of: 1) finding a phenomenological function to reproduce the measured total magnetization as the sum of independent contributions (populations) from different NWs whose magnetization projection can only be DP or RP as a function of *H*, 2) following the dispersion relation for the DP (RP) branch that corresponds to the full-line (dash-line) of Fig. 6-L2, with its population as a function of *H*; 3) adding algebraically the two contributions centered at their natural frequencies.

The agreement is very good for L-Band, excellent in DP X-Band, and good in RP X-Band, considering the simplicity of the model. For Q-Band it indicates not difference between DP and RP should be expected, in accordance with experiment. Only coherent rotation has been considered in this model. Other mechanisms that could contribute to the microwave absorption in the irreversible region have not been taken into account.

4. Conclusion

In this chapter we have reviewed some of the characteristics of Ni ferromagnetic nanowires grown by electrodeposition into AAO membranes of very good uniformity. A uniaxial anisotropy model was detailed and some results of FMR were show to be consistent with small variations in the filling factors indicating dipolar interactions compete with the uniaxial character of the magnetic anisotropy. Furthermore, the measured filling factors indicate small variations in the magnetic anisotropy between samples could be associated with these subtle structural changes in the AAO matrix. We showed that a contribution to the FMR line-widths can be originated in fluctuations in the porosity or filling factors of the sample, particularly in the condition *H//*NW. On the other hand, local distortions from the cylindrical shape would affect more strongly the line-width in the perpendicular condition.

The most important result of this work is that there is *no blocking in ferromagnetic resonance* in the way in which is normally used in AC susceptibility, essentially because FMR is not performed at *H* = 0. In many cases the applied field is higher than the irreversibility field (Fig. 4) and this condition defines a single energy minimum, therefore the system will be performing small oscillations around this minimum because the magnetization tends to relax extremely fast to the equilibrium position [Kittel, 2005]. What many researchers have believed (ourselves included in the past! [Sánchez *et al.*, 1999]) to be caused by "blocking" can be explained as being caused by the effective anisotropy field as a function of temperature growing larger than the characteristic exciting frequency, ω/γ, and thus not being able to excite resonantly the material at any applied field. In this sense the Ni NW are

an excellent system to study the response far above (Q-Band), above and near (X-Band), and below (L-Band) the anisotropy field gap.

5. Acknowledgment

6. References

Allende, S. Altbir, D. Salcedo, E. Bahiana & M. Sinnecker, J. P. ,(2008) Propagation of transverse domain walls in homogeneous magnetic nanowires, *Journal of Applied Physics*, vol 104, No 1 (June 2008) pp 013907-1/6, ISSN: 0021-8979.

Antoniak, C. , Lindner, J. & Farle, M. (2005), Magnetic anisotropy and its temperature dependence in iron-rich Fe_xPt_{1-x} nanoparticles *Europhysics Letters* Vol 70, No 2 (March 2005) pp 250-256, ISSN: 0295-5075.

Berger, R. , Bissey, J-C., Kliava, J. , Daubric, H. & Estournès, C. (2001), Temperature dependence of superparamagnetic resonance of iron oxide nanoparticles, *Journal of Magnetism and Magnetic Materials*, Vol 234, No 3 (September 2001) pp. 535-544, ISSN: 0304-8853.

Boucher, V., & Ménard, D. (2010), Effective magnetic properties of arrays of interacting ferromagnetic wires exhibiting gyromagnetic anisotropy and retardation effects, *Physical Review B* Vol 81, No 17 (May 2010) pp 174404-1/21, ISSN: 0163-1829.

Brown, J. W. (1963), Thermal fluctuations of a single-domain particle, *Physical Review* 130, No 5 (June 1963), pp. 1677-1686, ISSN: 0031-899X.

Casanova, F., Chiang, C. E., Li, C-P., Roshchin, I. V. , Ruminski, A. M., Sailor M. J., and Schuller, I. K. (2008); Gas adsorption and capillary condensation in nanoporous alumina films *Nanotechnology*, Vol. 19, No.31 (June 2008) pp. 315709-1/6, ISSN: 0957-4484.

Cullity, B. D., 1972, *Introduction to Magnetic Materials*, pp. 618-620. Addison Wesley. Readding, Massachusetts, USA, ISBN: 0-201-01218-9.

Darques, M., Spiegel, J., De laTorre Medina, J., Huynen, I., & Piraux, L. (2009), Ferromagnetic NW-loaded membranes for microwave electronics *Journal of Magnestims and Magnetic Materials*, Vol. 321, No. 14 (July 2009) pp. 2055–2065, ISSN: 0304-8853.

Darques, M., De la Torre Medina, J., Piraux, L., Cagnon L. & Huynen, I., Microwave circulator based on ferromagnetic NWs in an alumina template *Nanotechnology* Vol 21, No14 (March 2010) pp. 145208-1/4, ISSN: 0957-4484.

De Biasi, E., Ramos, C. A. & Zysler, R.D. (2003), Size and anisotropy determination by ferromagnetic resonance in dispersed magnetic nanoparticle systems *Journal of Magnetism and Magnetic Materials*, Vol 262, No 2, (Jun 2003) pp. 235-241; Vol 278, No 1-2, (Jul 2004), pp 289. ISSN: 0304-8853.

De Biasi, E., Ramos, C.A., Zysler, R.D., Romero, H. (2004), Ferromagnetic resonance in amorphous nanoparticles *Physica B*, Vol 354, No 1-4 (Dec 2004) pp. 286-289. ISSN: 0921-4526.

De Biasi, E., Zysler, R. D., Ramos, C. A., Romero, H. & Fiorani, D. (2005) Surface anisotropy and surface-core interaction in Co-Ni-B and Fe-Ni-B dispersed amorphous nanoparticles *Physical Review B* Vol 71, No 10 (Mar 2005) pp. 104408-1/6, ISSN: 0163-1829.

De Biasi, E., Zysler, R.D., Ramos, C. A. & Knobel, M. (2008), A new model to describe the crossover from superparamagnetic to blocked magnetic nanoparticles *Journal of Magnetism and Magnetic Materials*, Vol 320, No 14, (Jul 2008) pp. e312-e315. ISSN: 0304-8853.

De La Torre Medina, J., Piraux, L., Olais Govea, J. M. & Encinas, A. (2010) Double ferromagnetic resonance and configuration-dependent dipolar coupling in unsaturated arrays of bistable magnetic NWs *Physical Review B*, Vol 81, No 14 (Apr 2010) pp. 144411-1/11, and references there in, ISSN: 1098-0121.

Dorman, J.L., Fiorani, D. & Tronc, E. (1997), Magnetic relaxation in fine-particle systems *Advances in Chemical Physics* Vol 98 (Jan 1997) pp. 283-494, ISBN: 0-471-16285-X.

Ebels, U., Duavil, J.-L., Wigen, P. E., Piraux, L., Buda, L. D., Ounadjela, K. (2001), Ferromagnetic resonance studies of Ni nanowire arrays, *Physical Review B*, Vol 64, No 14 (Sep 2001), pp.14421-1/6, ISSN: 1098-0121.

Encinas-Oropesa, A., Demad, M., Piraux, L., Huynen, I. & Ebels, U. (2001) Dipolar interactions in arrays of nickel NWs studied by ferromagnetic resonance, *Physical Review B*, Vol 63, No 10 (February 2001) pp 104415-1/6, ISSN: 1098-0121.

Ennas, G. , Musinu, A., Piccaluga, G., Zedda, D.,Gatteschi, D., Sangregorio, C. , Stanger, J. L., Concas G. & Spano G. (1998), *Chemistry of Materials*, Vol(10), No 2, (Jan 1998), pp. 495-502, ISSN: 0897-4756.

Farle, M. (1998), Ferromagnetic resonance of ultrathin metallic layers. *Reports of Progress in Physics*, Vol 61, No 7, (Jul 1998), pp. 755-826, ISSN: 0034-4885.

Ferain, E., Legras, R. (2009), Templates for engineered nano-objects for use in microwave, electronic devices and biomedical sensing application, *Nuclear Instruments and Methods Physics Research B* Vol. 267, No. 6, (Mar 2009),pp. 1028–1031, ISSN: 0168-583X.

Fert, A. (2008). Nobel Lecture: Origin, development, and future of spintronics. *Reviews of Modern Physics*, Vol. 80, No.4, (Oct-Dec 2008), pp. 1517-1530, ISSN 0034-6861.

Fert, A., Piraux, L. (1999), Magnetic NWs *Journal of Magnetism and Magnetic Materials*, Vol. 200, No.1-3, (Oct 1999), pp. 338-358 ISSN: 0304-8853.

Hertel, R., Kirschner, J. (2004), Magnetization reversal dynamics in nickel NWs, *Physica B* Vol 343 No 1-4, (January 2004) pp., 206–210. ISSN: 0921-4526.

King, A. R., Mydosh, J. A., Jaccarino, V. (1986), ac Susceptibility Study of the d= 3 Random-Field Critical Dynamics, *Physical Review Letters* Vol 56, No 23 (Jun 1986) pp. 2525-2528. ISSN 0031-9007.

Kittel, C., 2005, *Introduction to Solid State Physics*, 8th Edition, pp 379-383J. Willey & Sons, Hoboken, NJ, USA, ISBN 0-471-41526-X

Kraus, L., Infante, G., Frait, Z. & Vázquez, M., (2011), Ferromagneticresonance in very thin wires (from micro- to nanowires), Physical Review B, Vol 83, No 17 (May 2011) pp 174438-1/11. ISSN 1098-0121.

Li, T., Sui, Y., Huang, Z., Yang, S., Gu, B. & Du Y. (2005) , Spin-configuration-related ferromagnetic resonance in nickel nanowire array, *Journal of Physics: Condensed Matter*, Vol 17, No 23, (May 2005) pp. 3637-3645. ISSN: 0953-8984

Likodimos, V., & Pissas, M. (2007), Phase coexistence and magnetic anisotropy in $La_{1-x}Ca_xMnO_3$ ($0<x\leq0.23$) studied via electron spin resonance *Physical Review B* Vol 76, No 2 (Jul 2007) pp. 024422-1/10pp. ISSN: 1098-0121.

Lubitz, P. Rubinstein, M., Christodoulides, J. A. & Chrisey D. B. (2004), Source of anomalies in the temperature dependence of ferromagnetic resonance and susceptibility data in the FeAg heterosystem, *Journal of Applied Physics*, Vol 95, No 11 (June 2004) pp. 7124-7126. ISSN: 0021-8979.

Lundgren, L., Svendlindh, P., Norblad, P. & Beckman, O. (1983), Dynamics of the Relaxation-Time Spectrum in a CuMn Spin-Glass, *Physical Review Letters*, Vol 51, No 10, (Setember 1983) pp. 911-914. ISSN: 0031-9007.

Masuda, H., Fukuda, K. (1995), Ordered Metal Nanohole Arrays Made by a Two-Step Replication of Honeycomb Structures of Anodic Alumina *Science*, Vol. 268, No 5216, (June 1995), pp. 1466-1468 ISSN: 0036-8075.

Morrish, A.H. (2001) *"Physical Principles of Magnetism"*, IEEE Press, Piscataway, New York, 2001. ISBN: 0-7803-6029-X.

Mydosh, J.A. (1993), *"Spin-glasses: an experimental introduction"*, Taylor & Francis, London, Great Britain (June 1993). ISBN: 10- 0748400389.

Nielsch, K., Müller, F., Li, A.-P. & Gösele, U., (2000) Uniform Nickel Deposition into Ordered Alumina Pores by Pulsed Electrodeposition, Advanced Materials, Vol 12, No 8, (April 2000), pp 582-586, ISSN: 0935-9648.

Nielsch, K., Wehrspohn, R., Barthel, J., Kirschner, J., Gösele, U., Fischer, S. Kronmüller, H. (2001), Hexagonally ordered 100 nm period nickel NW arrays, *Applied Physics Letters* Vol 79, No 9, (August 2001), pp. 1360-1362. ISSN: 0003-6951.

Orosco, M. M., Pacholski, C., Sailor, M. J. (2009) Real-time monitoring of enzyme activity in a mesoporous silicon double layer *Nature Nanotechnology*, Vol 4, pp. 255-258. ISSN: 1748-3387.

Pacholski, C., Yu, C., Miskelly, G. M., Godin, D., and Sailor, M. J. (2006), Relective Interferometric Fourier Transform Spectroscopy: A Self-Compensating Label-Free Immunosensor Using Double-Layers of Porous SiO_2 *Journal of the American Chemical Society*, Vol. 128, No 13, (Aug. 2006), pp. 4250-4252, ISSN: 0002-7863.

Pirota, K.R., Knobel, M., Hernandez-Velez, M., Nielsch K. & Vázquez, M. (2010) Magnetic Nanowires: fabrication and characterization, *Handbook of Nanoscience and Nanotechnology*, vol. II Eds. A. V. Narlikar and Y. Y. Fu (Oxford University Press, USA, 2010) chapter XXII, pp. 772-824, ISBN: 978-019-953305-3

Pirota, K.R., Navas, D., Hernández-Velez, M., Nielsch, K. & Vázquez, M. (2004) Novel magnetic materials prepared by electrodeposition techniques: arrays of nanowires and multi-layered microwires, Journal of Alloys and Compounds Vol. 369, No 1-2, (April 2004), pp 18-26, ISSN: 0925-8388

Pujada, B.R., Sinnecker, E.H.C.P., Rossi, A. M., Ramos, C. A. & Guimarães, A.P.(2003). FMR evidence of finite-size effects in CoCu granular alloys *Physical Review B*. Vol 67, No 2 (January 2003) pp. 024402-1/6, ISSN: 0163-1829.

Raikher, Yu.L., Stepanov, V.I. (1994) Ferromagnetic resonance in a suspension of single-domain particles *Physical Review B* Vol 50, No 9 (September 1994) pp. 6250- 6259, ISSN: 1098-0121.

Ramos, C. A., King, A. R. & Jaccarino, V. (1988), Determination of the crossover exponent in the random-field system $Mn_xZn_{1-x}F_2$, *Physical Review B* Vol 37, No 10 (April 1988), pp. 5483-5492 ISSN: 1098-0121.

Ramos, C. A., Vázquez, M., Nielsch, K., Pirota, K., Rivas, R. B., Wherspohn, R. B., Tovar, M., Sánchez, R. D. & Gösele, U. (2004a). FMR characterization of hexagonal arrays of Ni NWs. *Journal of Magnetism and Magnetic Materials* Vol 272–276 (May 2004) pp. 1652–1653. ISSN 0304-8853.

Ramos, C. A., Vassallo Brigneti, E. & Vázquez, M. (2004b). Self-organized NWs: evidence of dipolar interactions from ferromagnetic resonance measurements, *Physica B* Vol 354 (2004) pp. 195-197 ISSN: 0921-4526.

Ramos, C. A., De Biasi, E., Zysler, R.D., Vassallo Brigneti, E. & Vázquez, M. (2007) 'Blocking´ effects in magnetic resonance? The ferromagnetic NW case *Journal of Magnetism and Magnetic Materials*, Vol 316, No 2 (September 2007) pp. e63-e66 ISSN 0304-8853.

Sánchez, R. D., Rivas, J., López Quintela, A. M., González Penedo, A. , García Bastida, A.J., Ramos, C. A., Zysler, R.D.& Ribeiro Guevara, S. (1999), Magnetization and EPR of Co clusters embedded in Ag nanoparticles, *Journal of Physics: Condensed Mater*, Vol 11, No 29, (1999) pp. 5643-5654, ISSN 0953-8984.

Smit, J. & Beljers, H.G. (1955) Ferromagnetic resonance absorption in $BaFe_{12}O_{19}$, a highly anisotropic crystal, *Philips Research Reports* Vol 10, No 2 (April 1955)pp. 113-130, ISSN: 0031-7918.

Tovar, M., Causa, M. T., Ramos, C. A. & Laura-Ccahuana, D. (2008) Phase separation in La-Ca manganites: magnetic field effects. *Journal of Magnetism and Magnetic Materials*, Vol 320, No 3-4 (February 2008) pp.523-527, ISSN: 0304-8853.

Trunova, A. V., Linder, J., Meckenstock, R., Spasova, M., Farle, M., Ciuculescu, D., Amiens, C., Chaudret, B. & Respaud, M. (2009), Temperature dependent magnetic characterisation of core/shell $Fe_{80}Rh_{20}$ nanoparticles, *Journal of Magnetism and Magnetic Materials*, Vol 321, No 20 (Oct 2009), pp 3502-3506 ISSN: 0304-8853.

Vassallo Brigneti, E. C. (2009) Estudio de las propiedades estáticas y dinámicas de nanohilos magnéticos y películas nanoporosas, *Ph D. Thesis* (June 2009)pp 1-186, Instituto Balseiro, Universidad Nacional de Cuyo.

Vázquez, M., Hernández-Vélez, M., Pirota, K., Asenjo, A., Navas, D., Velásquez, J., Vargas, P. & Ramos, C. (2004) Arrays of Ni NWs in alumina membranes: magnetic properties and spatial ordering *European Physics Journal B*, Vol 40 No 4, (June 2004) pp. 489-497, ISSN: 1434-6028.

Vázquez, M., Ramos, C., Vassallo, E., Jaafar, M. & Asenjo, A. (2005), Combined Ferromagnetic Resonance and Magnetic Force Microsopy studies in arrays of magnetic NWs, *Transactions of the Magnetic Society of Japan* Vol 5, No 4 (2005) pp. 157-160, ISSN:1346-7948.

Winkler, E., Causa, M. T., Ramos, C. A. & De Biasi, E., (2004) ESR phase competition study of $Pr_{0.5}(Ca_{0.85}Sr_{0.15})_{0.5}MnO_3$ *Physica B*, Vol 354, No 1-4 (December 2004), pp 51-54. ISSN: 0921-4526

Winkler, E., Causa, M. T. & Ramos, C. A. (2007), Ferromagnetic resonance study in $Pr_{0.5}(Ca_{1-x}Sr_x)_{0.5}MnO_3$, *Physica B* Vol 398, No 2, (September 2007) pp 434-437 ISSN: 0921-4526.

Yang, P., Yan, R. & Fardy M. (2010), Semiconductor Nanowire: What's Next?, *Nano Letters* Vol 10, No 5, (April 2010) pp 1529–1536, ISSN: 1530-6984.

Nanowires - Fundamental Research

Edited by Dr. Abbass Hashim

Understanding and building up the foundation of nanowire concept is a high requirement and a bridge to new technologies. Any attempt in such direction is considered as one step forward in the challenge of advanced nanotechnology. In the last few years, InTech scientific publisher has been taking the initiative of helping worldwide scientists to share and improve the methods and the nanowire technology. This book is one of InTech's attempts to contribute to the promotion of this technology.

How to reference

In order to correctly reference this scholarly work, feel free to copy and paste the following:

Carlos A. Ramos, Ettore Vassallo Brigneti, Emilio De Biasi and Manuel Vázquez (2011). On the behavior of Ni Magnetic Nanowires as studied by FMR and the effect of "blocking"., Nanowires - Fundamental Research, Dr. Abbass Hashim (Ed.), ISBN: 978-953-307-327-9, InTech, Available from:

http://www.intechopen.com/books/nanowires-fundamental-research/on-the-behavior-of-ni-magnetic-nanowires-as-studied-by-fmr-and-the-effect-of-blocking-

INTECH

open science | open minds